Joule

CellPress

Article

Titanium-Perovskite-Supported RuO_2 Nanoparticles for Photocatalytic CO_2 Methanation

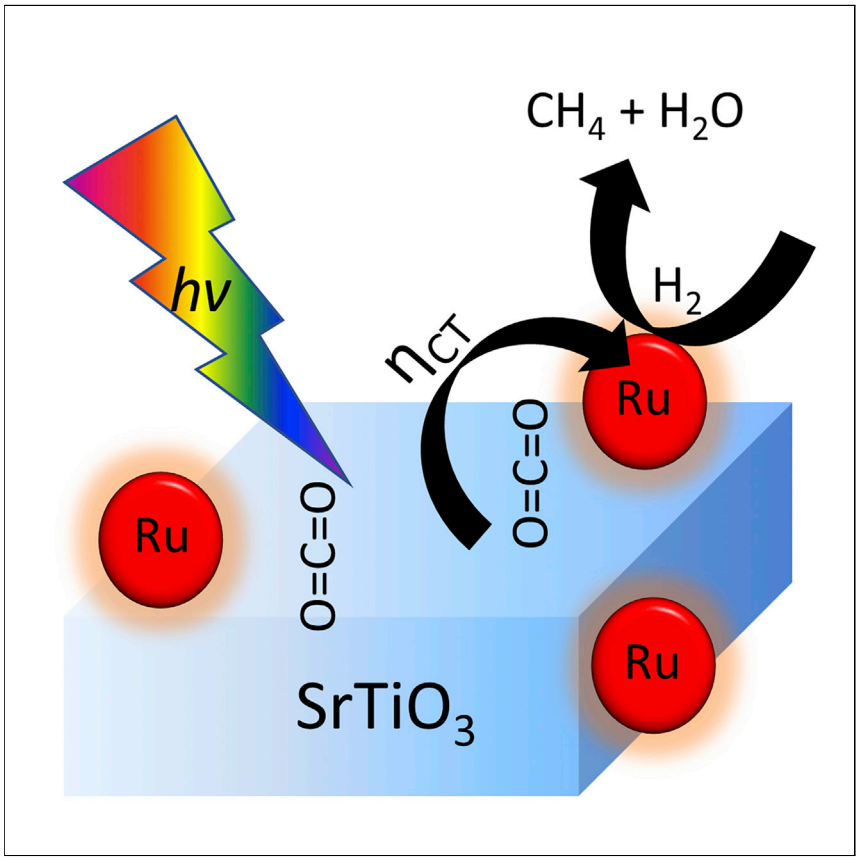

RuO_2 nanoparticles supported on strontium titanate (STO) have demonstrated outstanding photothermal activity for CO_2 methanation operating at 150°C under simulated sunlight irradiation. The photoresponse of the material is mainly due to UV photons, although RuO_2/STO still retains about 50% efficiency under visible light irradiation (>400 nm). Mechanistic studies are compatible with a photothermal process with minor contribution of photocatalytic electron/hole charge separation. This value ranks the material among the most efficient methanation photocatalysts.

Diego Mateo, Josep Albero, Hermenegildo García

hgarcia@qim.upv.es (H.G.)
joalsan6@itq.upv.es (J.A.)

HIGHLIGHTS

RuO_2 on $SrTiO_3$ exhibits outstanding photothermal activity for CO_2 methanation

The photothermal process exhibits a CH_4 production rate of 14.6 mmol CH_4 h^{-1} g^{-1}

The response of this material presents about 50% efficiency under visible light

The photocatalyst is efficient enough to operate also under continuous flow conditions

Mateo et al., Joule 3, 1–14
August 21, 2019
https://doi.org/10.1016/j.joule.2019.06.001

Please cite this article in press as: Mateo et al., Titanium-Perovskite-Supported RuO_2 Nanoparticles for Photocatalytic CO_2 Methanation, Joule (2019), https://doi.org/10.1016/j.joule.2019.06.001

Joule

CellPress

Article

Titanium-Perovskite-Supported RuO_2 Nanoparticles for Photocatalytic CO_2 Methanation

Diego Mateo,[1] Josep Albero,[1,*] and Hermenegildo García[1,2,*]

SUMMARY

This manuscript reports the photothermal activity for CO_2 methanation of RuO_2 nanoparticles supported on strontium titanate (STO) operating at 150°C under simulated sunlight irradiation. The RuO_2/STO sample having the optimal performance exhibits under ultraviolet-visible (UV-vis) irradiation with a power of 108 mW/cm^2 at 150°C a CH_4 production rate of 14.6 mmol CH_4 h^{-1} g^{-1}. The photoresponse of the material is mainly due to UV photons, although RuO_2/STO still retains about 50% efficiency under visible light irradiation (>400 nm). Mechanistic studies are compatible with a photothermal process with minor contribution of photocatalytic electron-hole pair charge separation. The photocatalyst is efficient enough to also operate under continuous flow conditions, achieving with a contact time of 3 s at 150°C under about 1 sun irradiation a steady-state CH_4 production rate of 30 μmol h^{-1} for an 8-h-long experiment. This value ranks the material among the most efficient methanation photocatalysts.

INTRODUCTION

Currently, there is much interest in developing novel processes to transform CO_2 into fuels or chemicals since in this way, atmospheric CO_2 emissions could be decreased.[1–3] Considering that CO_2 hydrogenations are among the few thermodynamically downhill reactions having CO_2 as a reagent, many studies have focused on this reaction.[4–6] Due to slow kinetics, hydrogenation of CO_2 can be carried out catalytically at temperatures above 250°C and, depending on the catalyst, even at higher temperatures, typically about 550°C. Otherwise, the reaction rate of CO_2 hydrogenation would be unsatisfactorily low.[7–9] However, performing catalytic reactions at high temperatures requires the consumption of energy. In this regard, recent strategies that are attracting much interest consist of developing electrochemical CO_2 reduction in gas phase and aqueous media using the renewable electricity when produced in excess, as well as photoassisted versions of CO_2 hydrogenation, using solar light as an irradiation source[10–17] It has been found that photoassisted CO_2 hydrogenation can be carried out at much lower temperatures than conventional catalytic reactions. At those low temperatures, the thermal process either does not occur at all or contributes in a minor proportion to the CO_2 conversion.[11,18–20]

Regarding precedents of photoassisted CO_2 hydrogenation, it has been reported that Ru nanoparticles (NPs) deposited on silicon nanowires are a photothermal catalyst to produce CO_2 methanation, reaching a conversion rate of about 1 mmol/g·h at 150°C.[21] Under these conditions, reactions carried out without illumination showed thermal conversion of about 0.51 mmol/g·h.[21] Mechanistic studies have suggested

Context & Scale

The present study reports the CO_2 transformation to methane using RuO_2 nanoparticles supported on strontium titanate (STO), operating at 150°C under simulated sunlight irradiation. The RuO_2/STO sample having the optimal performance exhibits complete CO_2 conversion to methane in less than 2 h, probably the highest activity reported up to now. The photoresponse of the material is mainly due to UV light, although RuO_2/STO still retains about 50% efficiency under visible light irradiation. This result opens the possibility to use direct sunlight to transform the undesired atmospheric CO_2 into fuels, contributing to a neutral carbon footprint. The photocatalyst is efficient enough to also operate under continuous flow conditions, which makes this photocatalyst very attractive for industrial purposes.

Please cite this article in press as: Mateo et al., Titanium-Perovskite-Supported RuO_2 Nanoparticles for Photocatalytic CO_2 Methanation, Joule (2019), https://doi.org/10.1016/j.joule.2019.06.001

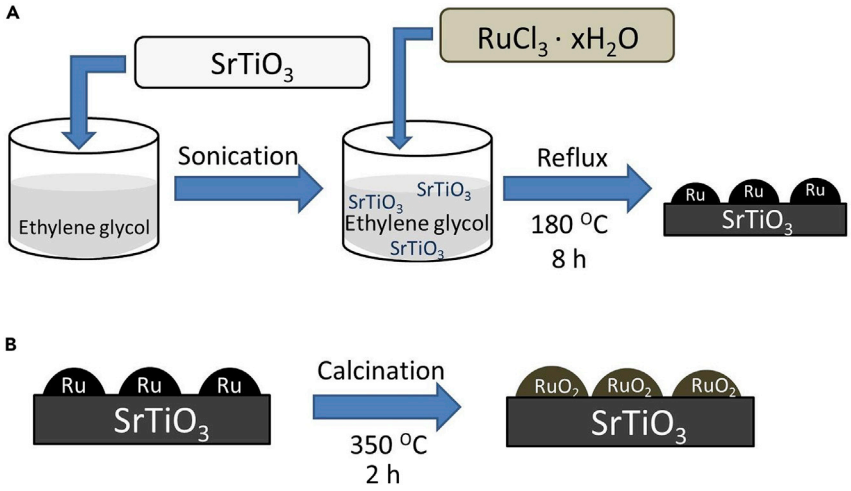

Scheme 1. RuO_2/STO Photocatalyst Preparation

(A) STO dispersion in ethylene glycol and Ru^{3+} impregnation and chemical reduction.

(B) Ru/STO calcination in air conditions.

that in the case of Ru NPs on silicon nanowires, the reaction involves light absorption by a narrow bandgap silicon semiconductor that, upon charge recombination, transfers the heat locally at the nanoscale to the Ru NPs, providing sufficient energy to catalyze the reaction.[22] Continuing with this line of research, it is important to develop more efficient photocatalytic systems able to activate the photothermal CO_2 hydrogenation at higher rates.

There exist in the literature precedents reporting that strontium titanate (STO) perovskite combined with co-catalysts, and suitable doping is a highly efficient photocatalyst to promote overall water splitting and dye degradation.[23–25] However, up to now, and as far as we know, there are no reports in the literature using STO-based photocatalytic systems to promote CO_2 conversion, particularly photoassisted CO_2 reduction by hydrogen. However, it seems that efficient charge migration from STO to metal NPs could be the basis for an efficient photocatalytic methanation process as well.

In the present manuscript, it is reported that RuO_2 NPs deposited on a Ti perovskite is a highly efficient photocatalyst to promote the light-assisted methanation of CO_2 at almost complete conversion at temperatures as low as 150°C. Available catalytic data support a reaction mechanism involving charge separation in the perovskite semiconductor as the key event leading to activation of the reaction.

RESULTS AND DISCUSSION

Photocatalyst Characterization

A commercial sample of STO was modified by depositing Ru NPs by impregnation that subsequently were oxidized by exposure to ambient atmosphere at 350°C. The preparation procedure is illustrated in Scheme 1.

The successful formation of RuO_2 on STO was determined by X-ray diffraction (XRD) (Figure 1), where the characteristic diffraction peaks corresponding to STO and RuO_2 were observed. The XRD patterns of RuO_2 and STO have also been acquired, and they are presented in Figure S1. As can be observed, the XRD pattern of the RuO_2/STO photocatalyst is the combination of its individual components.

[1]Instituto de Tecnología Química CSIC-UPV, Universitat Politécnica de Valencia, Valencia 46022, Spain

[2]Lead Contact

*Correspondence: hgarcia@qim.upv.es (H.G.), joalsan6@itq.upv.es (J.A.)

https://doi.org/10.1016/j.joule.2019.06.001

Please cite this article in press as: Mateo et al., Titanium-Perovskite-Supported RuO_2 Nanoparticles for Photocatalytic CO_2 Methanation, Joule (2019), https://doi.org/10.1016/j.joule.2019.06.001

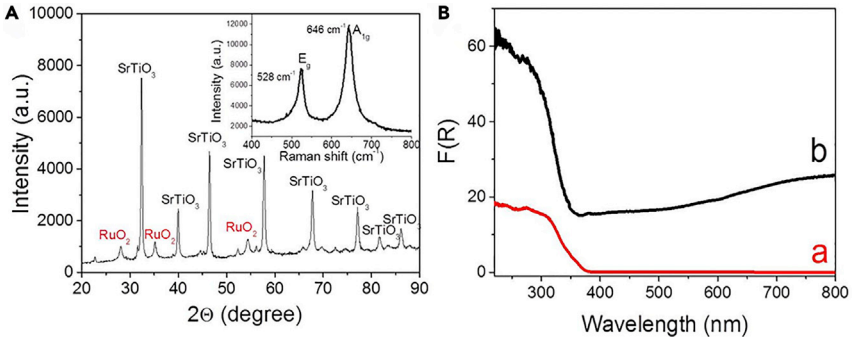

Figure 1. Photocatalyst Spectroscopic Characterization

(A) XRD pattern of RuO_2/STO photocatalyst (0.4 wt % Ru loading). The peaks corresponding to either RuO_2 or STO have been indicated. The inset shows the Raman spectrum of RuO_2/STO (0.4 wt % Ru loading) recorded upon 512 nm laser excitation.

(B) Diffuse reflectance UV-vis spectra, plotted as the Kubelka-Munk function of the reflectance (R) of (A) STO (red) and (B) RuO_2/STO (0.4 wt % Ru loading) (black).

Three samples at different RuO_2 loadings were prepared by changing the amount of $RuCl_3$ present in the preparation method. ICP-OES analysis of the samples determined that the Ru content of the three RuO_2/STO photocatalysts was 0.1, 0.4, and 1.2 wt % (weight percent), respectively.

The presence of these small amounts of RuO_2 on the fresh samples could be also confirmed by Raman spectroscopy, where the two characteristic E_g and A_{1g} bands corresponding to RuO_2 appeared at 528 and 646 cm^{-1}, respectively (inset Figure 1).

Deposition of RuO_2 on STO can also be monitored by diffuse reflectance ultraviolet-visible (UV-vis) absorption spectroscopy, where, in addition to the UV band characteristic of STO, the appearance of a broad absorption band spanning from 400 to beyond 800 nm due to the RuO_2 plasmon band was also recorded (Figure 1).[26]

The presence of RuO_2 was also observed by high-resolution transmission electron microscopy (HRTEM) (Figure 2), allowing the measurement of the particle size distribution. These images showed larger particles (30–80 nm) corresponding to STO on which the presence of much smaller NPs decorating STO surface can be observed. HRTEM images of these NPs allow the measurement of an interplanar distance of 0.17 nm that agrees well with the 211 interplanar distance in RuO_2. Statistical counting of a relevant number of RuO_2 NPs indicates that the average particle size is about 4.7 ± 1.1 nm, with a distribution between 2 and 7 nm (inset Figure 2). Energy dispersive X-Ray spectroscopy (EDS) analysis of these NPs confirmed that they are constituted by Ru, while the larger particles contain Sr and Ti (Figure S2).

Photocatalytic Activity

Photoassisted CO_2 hydrogenation was carried out in the gas phase in a sealed quartz photoreactor equipped with a heating ribbon controlling the temperature with a thermocouple in contact with the reactor walls. Independent measurements with an infrared thermometer focused on the photocatalyst bed during irradiation confirmed the correct operation of the heating system controlling the temperature of the bed during the time of the photocatalytic tests under the various irradiation wavelengths, with a discrepancy between the set point and the temperature of the infrared camera lower than 5°C. Illumination of the system was carried out from the top at a distance of 6 cm using the output of a 300 W UV-vis Xe lamp.

Please cite this article in press as: Mateo et al., Titanium-Perovskite-Supported RuO_2 Nanoparticles for Photocatalytic CO_2 Methanation, Joule (2019), https://doi.org/10.1016/j.joule.2019.06.001

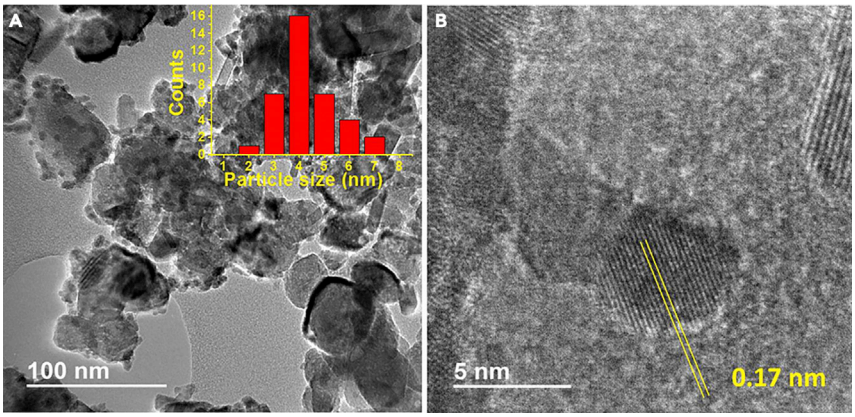

Figure 2. HRTEM Images of the RuO_2/STO Photocatalyst

(A) Representative image of RuO_2 NPs decorating the larger STO NPs (0.4 wt % Ru loading). The inset shows the size distribution histogram of the RuO_2 NPs. Scale bar, 100 nm.

(B) Magnified image of a RuO_2 NP indicating the interplanar distance in yellow lines. Scale bar, 5 nm.

The only product observed in all the photocatalytic experiments was CH_4, with CO as well as CH_3CH_3 or higher hydrocarbons being below the detection limit. The photocatalytic activity at 150°C of the three samples containing different loadings of Ru is presented in Figure 3.

As can be seen in Figure 3, there is an optimal amount of Ru to obtain the highest photocatalytic activity, with the efficiency of the photocatalyst decreasing at lower or higher Ru loadings. This optimal amount can be interpreted as a consequence of the combination of two opposite effects. On one hand, the photocatalytic activity should increase with the loading of Ru as active sites. On the other hand, excessive amount of Ru can result in larger and, therefore, less efficient Ru NPs. To support this proposal, HRTEM images of the three photocatalysts were acquired. The RuO_2 NP average size was calculated for each sample after measurement of a statistically relevant number of NPs (see Figure S3). It can be observed that from 0.1 to 0.4 wt % of Ru, the average particle size was very similar at about 4.7 nm, while the number of NPs in an image frame was increased significantly with loading. However, for 1.2 wt % of Ru the average particle size increased to 7.3 $\pm$ 1.8 nm. Under the present reaction conditions, RuO_2/STO with a Ru content of 0.4% was the most efficient photocatalyst in the series since it was the sample with the highest Ru loading but maintaining a low average particle size. All subsequent studies were carried out with this sample.

Figure 3 shows that a high conversion rate is achieved for the RuO_2/STO sample with optimal loading upon 1,080 W/m^2 irradiation and 150°C, reaching 9.6 mmol/g of total photocatalyst in the first 30 min. Even higher CO_2 conversion of about 90% of the initial CO_2 amount was accomplished under these conditions after a 2 h reaction, as can be observed in the inset of Figure 3.

The influence of the reaction temperature on the photocatalytic CO_2 methanation from room temperature up to 150°C was determined. It is worth noting that the correct operation of the heating system and the temperature value of the photocatalytic bed during irradiation were confirmed by an infrared thermometer with discrepancies smaller than 5°C. It was observed that CO_2 conversion upon irradiation without electrical heating (~50°C) was 1.5% at 2 h irradiation, increasing the CO_2 conversion and concomitantly the CH_4 formation as the reaction temperature

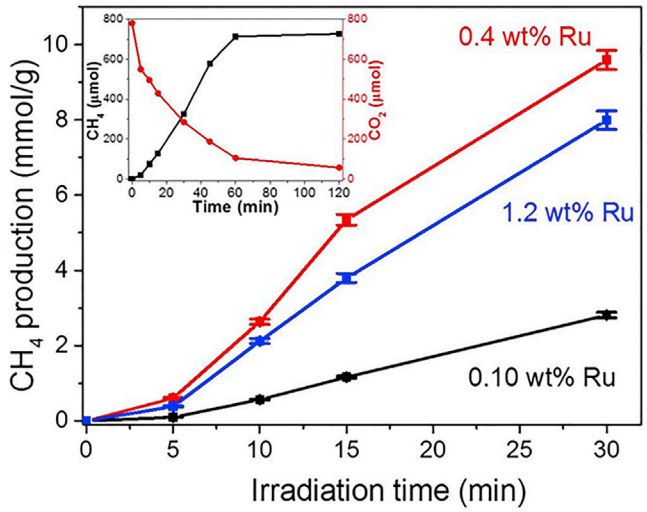

Figure 3. Photocatalytic Activity

CH_4 temporal profile (mmol/g) at 150°C obtained under (1,080 W/m^2) irradiation of the three samples containing different Ru loadings. The inset shows the CO_2 and CH_4 evolution (μmol) using the sample of 0.4 wt % Ru at 150°C upon illumination with a 300 W xenon lamp (1,000 W/m^2). Reactions conditions: 50 mg RuO_2/STO photocatalysts; P_{H2}: 1.05 bar, P_CO_2: 0.25 bar. Error bars indicate SD.

increases. Some of the data obtained are presented in Figure 4. When working at 150°C, very high CO_2 conversion (89.5%) was already achieved under our experimental conditions in 1 h irradiation time. Since 100°C represents a good balance between CO_2 conversion and lack of thermal reaction, subsequent experiments were carried out preferentially at this temperature.

In order to elucidate the role of STO in the RuO_2/STO photocatalyst, a control experiment using bare STO, without RuO_2 NPs, was carried out under the methanation conditions (100°C and 1,080 W/m^2). However, a CH_4 production four orders of magnitude lower than that of RuO_2/STO was obtained, pointing to the RuO_2 NPs as the active species. In a similar way, RuO_2 nanoparticles were used as a photocatalyst under identical reaction conditions (100°C and 1,080 W/m^2). In this case, 35 μmol CH_4/g were obtained after 2 h reaction, indicating that STO is not only acting as a support but has an important role in the methanation reaction promoting photoinduced charge separation and dramatically increasing the efficiency of the process.

Further investigation of the STO role was conducted replacing the STO by another related semiconductor material, such as commercial P25 TiO_2 NPs, and an insulator, such as Al_2O_3 NPs, as substrates of the RuO_2 NPs. The RuO_2/P25 and RuO_2/Al_2O_3 samples were prepared following an analogous procedure to that previously described for the RuO_2/STO sample. The XRDs of RuO_2/P25 and RuO_2/Al_2O_3 samples are presented as Figure S4. These XRD patterns confirm the presence of RuO_2 and TiO_2 as well as RuO_2 and Al_2O_3 in the RuO_2/P25 and RuO_2/Al_2O_3 samples, respectively.

The photocatalytic activities of RuO_2/STO, RuO_2/P25, and RuO_2/Al_2O_3 for methanation were compared. The results are presented as Figure S5. As can be observed, the CH_4 production using the RuO_2/STO photocatalyst was higher than that of RuO_2/P25 and RuO_2/Al_2O_3 samples. This comparison indicates that STO is not only acting

Please cite this article in press as: Mateo et al., Titanium-Perovskite-Supported RuO_2 Nanoparticles for Photocatalytic CO_2 Methanation, Joule (2019), https://doi.org/10.1016/j.joule.2019.06.001

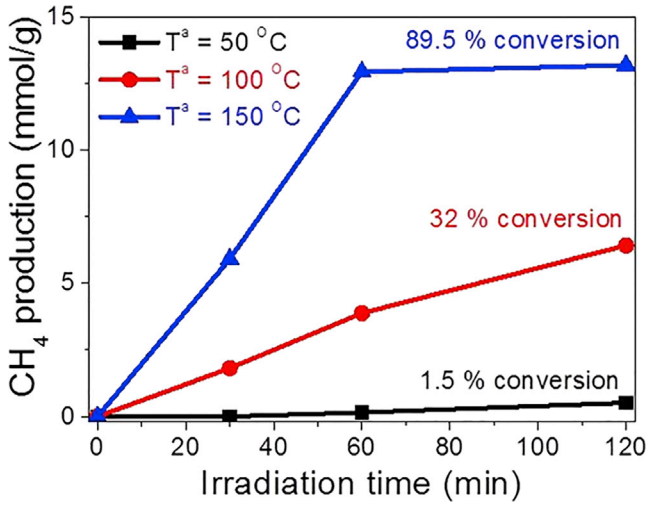

Figure 4. Temperature Influence in Photocatalytic Activity

Time-CH_4 production (mmol/g) plot under constant 1,080 W/m^2 illumination with a 300 W xenon lamp at 50°C (black squares, no electrical heating), 100°C (red dots), and 150°C (blue triangles). The final CO_2 conversion is indicated in each case. Reactions conditions: RuO_2/STO photocatalyst = 50 mg (Ru content 0.4 wt %); P_{H2}: 1.05 bar, P_CO_2: 0.25 bar.

as a support of the RuO_2 NPs but also plays an important role increasing the efficiency of the photoassisted methanation under the present conditions. The specific BET surface area values of STO and titania P25 were measured, obtaining 46 and 71 m^2/g, respectively. It is worth noticing that in spite of the smaller surface area of RuO_2/STO photocatalyst than that of RuO_2/P25, RuO_2/STO still presented enhanced photocatalytic performance for this reaction under the reaction conditions (Figure S5). Therefore, the origin of the improved activity of RuO_2/STO cannot be attributed to surface area effects. CO_2 adsorption measurements were performed in RuO_2/STO and RuO_2/P25 samples in order to evaluate the CO_2 adsorption capacity of these samples. As can be observed in Figure S6, the RuO_2/STO presents higher CO_2 adsorption capacity per surface unit than the RuO_2/P25. Therefore, the superior photocatalytic activity of RuO_2/STO over the RuO_2/P25 photocatalysts could be explained, at least in part, as derived from the higher CO_2 adsorption. The CO_2 adsorption and activation ability of Ti perovskites was already demonstrated before,[27] especially with regard to their ability to incorporate CO_2 in oxygen vacancies in the form of carbonate ions.

Regarding a quantitative evaluation of the light-assisted methanation, Ozin and coworkers have recently proposed that photothermal CO_2 methanation performance can be quantified as the product of both photochemical and thermal efficiencies by means of a photothermal figure of merit (*PTF*, Equation 1):

$$PTF(T) = \eta_{CT}(T^*)\ \alpha\ \frac{\kappa_{int}(T^*)\ T^*}{\kappa_{cat}(T^*)\ T}, \qquad \text{(Equation 1)}$$

where α is the solar absorptance, η_{CT}(T*) is the photochemical charge transfer efficiency at temperature T*, κ_{int} is the thermal conductivity of nanoheater, κ_{cat} is the thermal conductivity of the substrate, T* is the local temperature, and T is the measured temperature of the photocatalyst.

Since TiO_2 and $SrTiO_3$ materials present very similar absorbance and κ_{TiO2} and κ_{SrTiO3} are 11.8 and 12 W/mK, respectively, the only difference in PTF(T) for these

Please cite this article in press as: Mateo et al., Titanium-Perovskite-Supported RuO_2 Nanoparticles for Photocatalytic CO_2 Methanation, Joule (2019), https://doi.org/10.1016/j.joule.2019.06.001

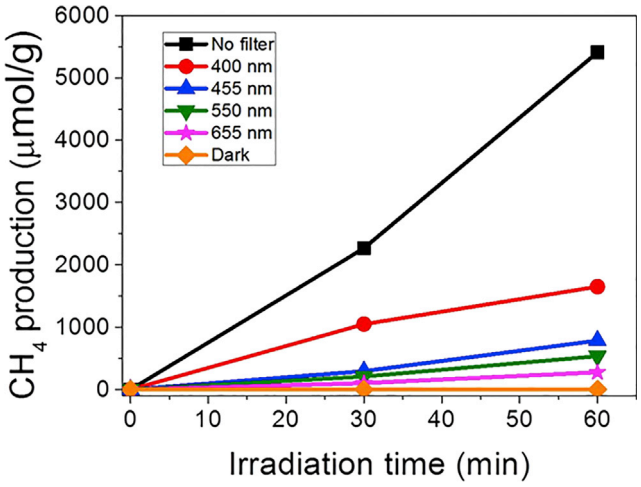

Figure 5. Spectral Response

Temporal CH_4 evolution (mmol/g) at 100°C under full illumination (1,080 W/m^2) from a 300 W xenon lamp, using different cutoff filters (from top to bottom in the figure: no filter or filter at 400, 455, 550, and 655 nm) as well as under dark conditions covering the photoreactor with aluminum foil and the lamp switched on. Reactions conditions: RuO_2/STO photocatalyst = 50 mg (Ru content 0.4 wt %); P_{H2}: 1.05 bar, P_CO_2: 0.25 bar.

two materials, justifying the higher efficiency of STO as support, should be the different $\eta_{CT}(T^*)$ values. Figure S7 shows an energy diagram based on reported values of the conduction and valence band energy of TiO_2 and STO semiconductors respect to Ru Fermi level. As can be observed there, $SrTiO_3$ presents 0.4 eV more reductive conduction band than TiO_2. This difference in ΔG^0 would be responsible of a better $\eta_{CT}(T^*)$ in STO than in TiO_2, thus explaining the improved activity in the photothermal CO_2 methanation.

Overall, the improved CH_4 production observed for RuO_2/STO photocatalyst with respect to RuO_2/P25 and RuO_2/Al_2O_3 is due to a combination of factors, including the superior CO_2 adsorption capacity, the photoresponsive semiconducting properties of TiO_2 and STO, and the higher $\eta_{CT}(T^*)$ of STO with respect to TiO_2.

This proposal about the role of STO in the high photothermal methanation activity of Ru NPs is supported by photoresponse measurements that indicate a large contribution of STO to the overall photocatalytic activity. Thus, the photoresponsiveness of the RuO_2/STO was determined at 100°C by using a series of cutoff filters. Notice that no changes in the temperature of the bed occur in spite of the differences in the photon flux since the heating system controls the reaction temperature. As commented earlier, the correct temperature control of the photocatalytic bed has been confirmed by infrared measurements. Under these conditions, a control experiment in the dark showed negligible CH_4 formation. The photoresponse measured with the full emission wavelength decreases as the excitation wavelength increases. The results obtained are presented in Figure 5. As can be seen there, the optimal RuO_2/STO sample exhibits some residual photocatalytic activity, even upon excitation at wavelengths above 655 nm, but it appears clear that the efficiency of short wavelength radiations and, particularly in the UV region where STO absorbs, is higher than those with long wavelengths. Taking into account the optical absorption spectrum of RuO_2/STO (Figure 1), the photoresponse can be interpreted as being derived from excitation of both the STO semiconductor and the Ru plasmon band, the former being more efficient with regard to promotion of the

photomethanation reaction by acting as the heater of Ru NPs. The relatively smaller contribution of RuO_2 to the photoresponse compared to STO is also in agreement with its low proportion in the photocatalyst.

Since photochemical reactions depend on light intensity, a series of experiments were carried out using the optimal photocatalyst at 100°C, varying the intensity of the light in the range from 1,080 to 1,321 W/m^2, observing that the evolution of CH_4 increases with the intensity of the light for experiments carried out at the same temperature (Figure S8).

It is worth commenting that just a small amount of RuO_2 NPs (about 0.4 wt %) supported on STO promoted a maximum CH_4 production rate of 14.5 mmol/g·h, referred to the total photocatalyst mass (Ru-STO), at 150°C and at about 1 sun irradiation (1,321 W/m^2) as reaction conditions. In related precedents, Jelle et al.[22] reported photocatalytic CO_2 methanation upon irradiation of RuO_2 NPs supported on 3D Si photonic crystals with concentrated light from a Xe lamp at 22,000 W/m^2 light intensity. Although the authors did not apply external heating, 150°C was measured as a consequence of the high-density irradiation and the infrared (IR) component from the Xe lamp. Even under these favorable conditions (particularly the high light flux), a CH_4 production rate of 4.4 mmol/g·h was obtained referring only to the Ru content (318 μg/cm^2).[22] Similarly, O'Brien et al.[28] also reported CO_2 methanation using Ru NPs spattered on black silicon nanowires upon irradiation with light intensities between 3,000 and 14,000 W/m^2 (150°C) achieving a CH_4 production rate of 10 mmol/g·h.[28] Our own group reported recently efficient photoassisted CO_2 methanation using Cu_2O NPs supported on defective graphene as photocatalysts under 1,000 W/m^2 light power and 250°C, obtaining a CH_4 production rate of 15 mmol/g·h.[29] Therefore, as far as we know, the RuO_2/STO material presented here appears to be among the most active photocatalysts described so far for CO_2 methanation operating at mild conditions; that is, at light flux irradiation close to 1 sun and low temperature. Moreover, complete CO_2 conversion can be achieved in 150 min using RuO_2/STO photocatalyst upon irradiation with 1,300 W/m^2 and 150°C.

Stability of RuO_2/STO as photocatalyst was determined by performing a series of consecutive photocatalytic methanation batch reactions with the same RuO_2/STO sample. The results in terms of reaction rate are presented in Figure 6. As can be seen there, the photocatalyst undergoes a notable decrease in photocatalytic activity from the first to the second use, as can be deemed by the decrease of methane production rate, but after that, subsequent reuses result in much lesser catalyst deactivation. However, during a given reuse test, CH_4 production rate remains constant. This gradual deactivation does not appear to be related to an increase in the average particle size of the RuO_2 NPs, as can be observed from HRTEM images of the four-times-used RuO_2/STO photocatalysts in Figure S9.

Another possibility could be that the observed deactivation is due to the deactivation of the photocatalyst active sites by CO. It has been previously reported that CO adsorption on Ru surfaces strongly affects H adsorption.[30] In order to provide evidence to support this hypothesis, a control experiment was carried out feeding the photoreactor with H_2 and CO, instead of CO_2, and submitting the CO and H_2 mixture to the usual methanation conditions (1,080 W/m^2 irradiation and 100°C) using a RuO_2/STO photocatalyst. The use of CO as substrate completely inhibited the methanation reaction under these conditions, this result being in agreement with the assumption that CO deactivates the photocatalyst active sites.

Please cite this article in press as: Mateo et al., Titanium-Perovskite-Supported RuO_2 Nanoparticles for Photocatalytic CO_2 Methanation, Joule (2019), https://doi.org/10.1016/j.joule.2019.06.001

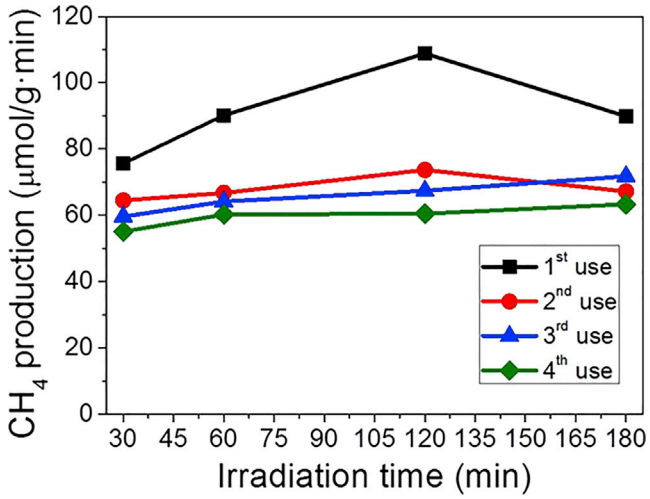

Figure 6. Photocatalyst Stability

CH_4 production rates (μmol/g·min) obtained from RuO_2/STO photocatalyst reused up to 4 times under illumination (1,000 W/m^2) with a xenon lamp of 300 W at 100°C. Note that the reaction rate is constant during each reuse, but the value decreases in the consecutive uses. Reactions conditions: RuO_2/STO photocatalyst = 50 mg (Ru content 0.4 wt %); P_{H2}: 1.05 bar, P_CO_2: 0.25 bar.

To gain some understanding on the Ru species in the photocatalytic CO_2 methanation promoted by RuO_2/STO, Raman measurements under Ar, H_2, and moisture were performed. As can be seen in Figure 3, the temporal profile of CH_4 evolution exhibits in a short time an induction period that could be attributable to the generation of the active Ru species during the photocatalytic reaction. To check this possibility, the Raman spectrum of the RuO_2/STO sample before the experiment was recorded under Ar atmosphere. Two vibration bands at 528 and 646 cm^{-1} corresponding to E_g and A_{1g} characteristic peaks of RuO_2 were recorded (see Figure 1), in agreement with the information provided by XRD about the presence of RuO_2 in the resting RuO_2/STO photocatalyst sample. When this sample is heated *in situ* at 100°C while flowing some H_2 through the cell, these Raman bands completely vanish. This change in the Raman spectrum indicates that RuO_2 has been fully reduced to metallic Ru that is silent in Raman spectroscopy. The conditions of this *in situ* measurement are, in principle, closely related to those under which the photocatalytic reaction takes place. After the complete disappearance of E_g and A_{1g} phonon peaks characteristic of RuO_2, the sample is exposed to air for 1 h at room temperature, and the appearance of E_a and A_{1g} peaks of characteristic RuO_2 are observed. Figure 7 shows a summary of these Raman measurements. These spectroscopic measurements indicate that upon exposure to H_2 at 100°C, RuO_2 becomes reduced to metallic Ru. Subsequent exposure to the air atmosphere again forms some RuO_2 within 1 h, indicating the reversibility of the oxidation-reduction cycle for the RuO_2/STO. Similar reversible behavior of Ru NPs has been reported in the literature. According to this, the most likely explanation of the induction period observed in the temporal profile of CH_4 evolution would be the reduction of most of the RuO_2 to metallic Ru that should be the active species present during CO_2 methanation. However, the partial re-oxidation of Ru nanoparticles by the CO_2 present in the reaction cannot be completely discarded, and thus, a non-stoichiometric RuO_x appears the most likely active site.

Analogous *in situ* experiments were carried out monitoring the X-Ray Photoelectron Spectroscopy (XPS) Ru 3d and 3p peaks under vacuum and after 1 h of heating at

Please cite this article in press as: Mateo et al., Titanium-Perovskite-Supported RuO_2 Nanoparticles for Photocatalytic CO_2 Methanation, Joule (2019), https://doi.org/10.1016/j.joule.2019.06.001

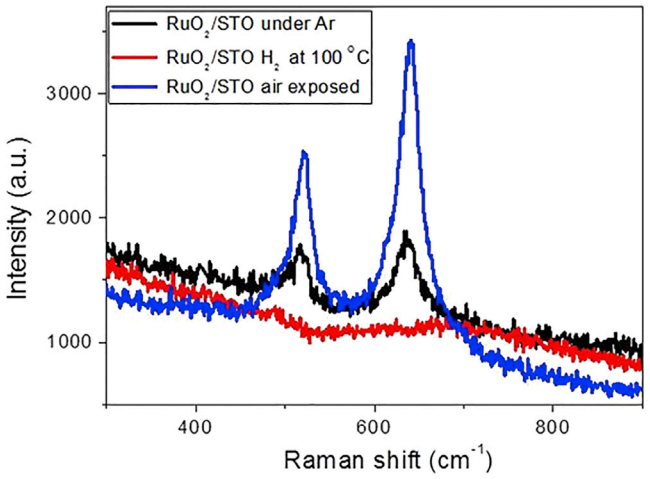

Figure 7. Active Site Determination

Raman spectra of a RuO_2/STO sample measured under Ar atmosphere (black), then submitted to H_2 flow at 100°C (red), and, finally, exposed to air conditions for 1 h (blue). Laser excitation: 512 nm.

100°C in H_2 atmosphere. Figure S10 presents a summary of these XPS measurements for RuO_2/STO, depending on the pre-treatment conditions. In this study, the 280.85 eV and 285.15 eV peaks assigned to Ru^{IV} 3d 5/2 and 3d 3/2, respectively, were shifted to lower binding energies (279.69 eV and 283.90 eV) corresponding to Ru^0, in accordance with the transformation of Ru^{IV} into lower oxidations states of Ru.[31] Since Ru 3d signals exhibits C 1s peaks interference, the Ru 3p core-levels of RuO_2/STO were also measured. As can be observed in Figures S10C and S10D, the binding energies of the Ru^{IV} 3p 3/2 component at 462.05 eV becomes shifted to 460.44 eV, corresponding to Ru^0 3p 3/2 upon H_2 treatment and is in good agreement with the observation based on the Ru 3d region.[31] Moreover, the Ti^{IV} 2p 3/2 and Ti^{IV} 2p 1/2 components at 458.95 eV and 464.58 eV, respectively, assigned to Ti in STO are also shown.[32] However, due to the severe overlap of the Ru signals with C and Ti peaks in XPS, a clear conclusion regarding the Ru oxidation state is difficult to prove using this technique.

Regardless of the oxidation state of Ru as either metallic or RuO_2, it should be mentioned that *in situ* UV-vis absorbance measurements of RuO_2/STO carried out at 100°C under continuous H_2 flow shows that the absorption spectrum of the photocatalysts does not undergo significant changes (see Figure S11). Therefore, it seems that the absorption spectra of RuO_2 and metallic Ru are similar and that light absorption is not influenced by the Ru oxidation state, and thus, similar photoresponses should be expected for Ru species regardless of the oxidation state.

Even though CO_2 as the origin of CH_4 in the previous photocatalytic reactions can be safely proved by the almost complete CO_2 conversion under some of the experimental conditions, additional experiments using isotopically labeled $^{13}C^{18}O_2$ were carried out, monitoring the product formation by mass spectrometry (MS). It should be commented that these conditions do not allow an efficient separation of the reaction mixture that is constituted by CH_4 and H_2O. Therefore, mass spectra contain simultaneously peaks corresponding to $^{13}CH_4$ and $H_2{}^{18}O$ (Figure S12). Equation 2 describes the expected formation of $^{13}CH_4$ and $H_2{}^{18}O$. Overall, the isotopic label measurements confirm the exclusive formation of $^{13}CH_4$ from $^{13}CO_2$ with no observation of $H_2{}^{16}O$ and no evidence of $^{12}CH_4$.

$$CO_2 + 4H_2 \rightarrow CH_4 + 2H_2O \qquad \text{(Equation 2)}$$

Please cite this article in press as: Mateo et al., Titanium-Perovskite-Supported RuO_2 Nanoparticles for Photocatalytic CO_2 Methanation, Joule (2019), https://doi.org/10.1016/j.joule.2019.06.001

As commented earlier, the superior performance of STO as support of Ru NPs derives in part from its photocatalytic activity. To further address the reaction mechanism of the photocatalytic CO_2 methanation using RuO_2/STO as photocatalyst, a series of experiments in the absence of H_2, but in the presence of two sacrificial electron donors with different oxidation potentials such as anisole (1.92 V versus Ag/$AgCl_{Sat.}$) and dimethylaniline (0.9 V versus Ag/$AgCl_{Sat.}$), were performed. If the reaction mechanism involved charge separation into conduction band electrons and valence band holes and subsequent chemical reduction of CO_2 by photogenerated conduction band electrons, the presence of electron donors should equally promote the methanation at a reaction rate that should correlate with the electron donor oxidation potential. In fact, very frequently, photocatalytic CO_2 reductions are carried out using triethanolamine and other electron donors, whereby the formation of CH_4, CO, or formate is observed.[33] It was observed that the presence of sacrificial electron donors gives rise to the formation of some CH_4 (see Figure S13). However, the formation rate of CH_4 in the presence of sacrificial electron donors is one order of magnitude lower than the conventional methanation experiments using H_2, even though these sacrificial electron donors should quench holes more efficiently than H_2. Thus, these quenching experiments indicate that although the photomethanation reaction can have some contribution by the photocatalytic mechanism involving charge separation and subsequent electron transfer from the semiconductor band to CO_2, most of the CH_4 formed should derive from a photothermal mechanism.

According to this mechanism, light excitation produces charge separation and recombination resulting in a local thermal effect at the catalytic Ru NPs. The local temperature should be high enough to promote the catalytic CO_2 methanation on Ru.

Finally, the RuO_2/STO photocatalytic activity was evaluated under continuous flow operation. Continuous flow photocatalytic methanation is mandatory if the process has to become commercial and performed on a massive scale. For this purpose, a total flow of 25 mL/min, containing 80% H_2 and 20% CO_2, was passed through a cylindrical quartz photoreactor containing 150 mg of a RuO_2/STO bed placed on a fritted glass filter. The contact time of CO_2 with the irradiated photocatalyst under our experimental conditions was estimated at 3.3 s. The photoreactor was heated at 150°C by means of an electrical heating ribbon controlled by a thermocouple, and the irradiation was carried out using a 300 W xenon lamp at 1,100 W/m^2. The setup of the photoreactor operating in continuous flow under illumination is shown in Supplemental Information (Figure S14). The CH_4 temporal evolution under continuous flow operation mode was followed for a period longer than 8 h (Figure 8), measuring at the beginning of the irradiation a maximum CH_4 formation rate of 122 μmol/h. This rate was decaying gradually up to 30 μmol/h during the first 3 h, indicating the occurrence of an initial deactivation pathway. After this period, the CH_4 production rate remained constant for at least 5 h. It seems that RuO_2/STO becomes stabilized after an initial period to a certain distribution of active sites that produces CH_4 at a rate stable over long periods.

The initial photocatalyst deactivation could be attributed to a certain degree of Ru NPs agglomeration under the reaction conditions. However, as previously commented when presenting the data of the four consecutive batch reuses, no relevant change in the particle size distribution was again observed in the continuous flow reaction, as can be observed in the HRTEM images presented in Figure S15. XRD analysis of the photocatalysts before and after the CO_2 methanation in continuous

Please cite this article in press as: Mateo et al., Titanium-Perovskite-Supported RuO_2 Nanoparticles for Photocatalytic CO_2 Methanation, Joule (2019), https://doi.org/10.1016/j.joule.2019.06.001

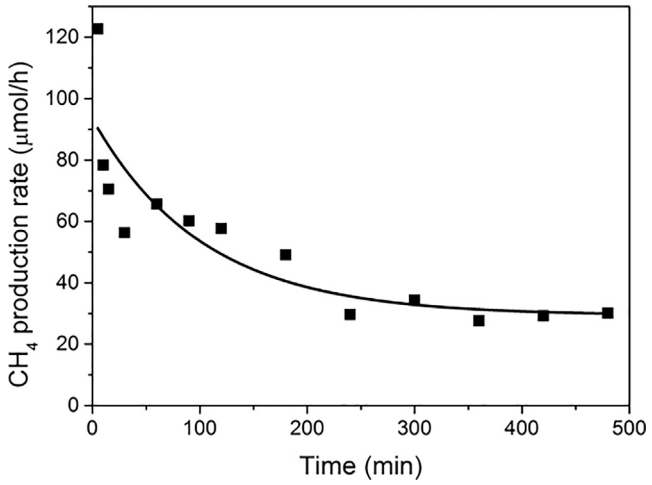

Figure 8. CH_4 Production Rate under Continuous Flow Operating Conditions

The line indicate CH_4 formation trend. CH_4 formation in continuous flow was measured using a total flow of 25 mL/min containing 80% of H_2 and 20% of CO_2. The photocatalyst amount was 150 mg. Light intensity 1,100 W/m^2. Temperature = 150°C.

flow confirmed that Ru^0 is the species present during the photocatalytic reaction (Figure S16). Therefore, CO poisoning seems to be the most reasonable photocatalyst deactivation process. In spite of this initial partial deactivation, the continuous flow operation provides valuable information about the stability of the catalytic active sites as a function of the time of stream.

In summary, a photothermal catalyst for CO_2 methanation based on Ru NPs supported on an STO semiconductor was prepared. The available activity data using simulated solar light indicate that the RuO_2/STO photocatalyst is among the most efficient materials for light-assisted methanation, reaching at 150°C a productivity of 14.5 mmol/g·h. This high efficiency of RuO_2/STO derives from a combination of factors, including high CO_2 adsorption capacity of STO, its semiconductor activity, and a more favorable charge transfer to metallic Ru NPs formed under the conditions of the reaction. The high activity of the optimized RuO_2/STO sample allows the performance of continuous flow photometanation, observed after an initial period a steady CH_4 production rate of 30 μmol/h. Mechanistic studies using sacrificial electron donors indicate that the contribution of a photocatalytic electron-hole separation to the photoreaction is minor. Overall, the results achieved, particularly those under continuous flow conditions, show the feasibility to move toward scale-up processes, trying to implement photothermal processes closer to commercial stages.

EXPERIMENTAL PROCEDURES

Photocatalyst Preparation

A suspension of $SrTiO_3$ (Aldrich) in ethylene glycol (5 mg/mL) was prepared by sonication at 700 W for 30 min. A certain amount of $RuCl_3 \cdot xH_2O$ (Acros Organics) was added to the reaction mixture and the reduction of Ru was performed at 180°C for 8 h under continuous stirring. Ru-containing STO samples were recovered by filtration and washed exhaustively with water and acetone. After drying at 100°C, samples were calcined under air at 350°C for 2 h to obtain the final RuO_2 nanoparticles supported on $SrTiO_3$.

Photocatalytic Measurements

50 mg of photocatalyst was loaded into a cylindrical quartz photoreactor equipped with a nickel alloy thermocouple connected to a heating ribbon and a temperature controller. The correct control of the temperature of the photocatalytic bed was confirmed by independent measurements with an RS PRO infrared thermometer RS127 focused on the photocatalyst bed. The discrepancy between the temperature setting point and the value of the infrared camera was lower than 5°C during the photocatalytic reactions. H_2 and CO_2 were introduced in a 4:1 molar ratio up to achieve a final pressure of 1.3 bar. The photoreactor was heated at different temperatures prior to irradiation and, when the desired temperature was stabilized, the photocatalyst was irradiated from the top (6 cm above) through fiber optics with UV-vis light from a 300 W Xe lamp. The evolved CH_4 was analyzed using a gas chromatograph (Agilent 490 MicroGC) equipped with two channels, both with TC detectors and Ar as the carrier gas. One channel has a molecular sieve of 5 Å column and analyzes H_2. The second channel has a Pore Plot Q column and analyzes CO_2, CO, and up to C_4 hydrocarbons. Quantification of the percentage of each gas was based on prior calibration of the system by injecting mixtures with known percentages of gases.

SUPPLEMENTAL INFORMATION

Supplemental Information can be found online at https://doi.org/10.1016/j.joule.2019.06.001.

ACKNOWLEDGMENTS

The authors thank the Spanish Ministry of Economy and Competitiveness (Severo Ochoa SEV2016-0683 and CTQ2015-69563-CO2-1) and Generalitat Valenciana (Prometeo 2017-083) for financial support. J.A. and D.M. also thank UPV for a postdoctoral scholarship and the Spanish Ministry of Science for a PhD scholarship.

AUTHOR CONTRIBUTIONS

D.M. prepared and characterized the materials and performed most of the experiments; J.A. supervised the experiments and wrote part of the manuscript; H.G. supervised the research and wrote most of the manuscript. All the authors discussed the results and corrected the article draft.

DECLARATION OF INTERESTS

The authors declare no competing interests.

Received: March 29, 2019
Revised: May 6, 2019
Accepted: May 31, 2019
Published: August 21, 2019

REFERENCES

1. Kondratenko, E.V., Mul, G., Baltrusaitis, J., Larrazábal, G.O., and Pérez-Ramírez, J. (2013). Status and perspectives of CO 2 conversion into fuels and chemicals by catalytic, photocatalytic and electrocatalytic processes. Energy Environ. Sci. *6*, 3112–3135.

2. Tahir, M., and Amin, N.S. (2013). Recycling of carbon dioxide to renewable fuels by photocatalysis: Prospects and challenges. Renew. Sust. Energ. Rev. *25*, 560–579.

3. Yuan, L., and Xu, Y.-J. (2015). Photocatalytic conversion of CO2 into value-added and renewable fuels. Appl. Surf. Sci. *342*, 154–167.

4. Wu, J., Wen, C., Zou, X., Jimenez, J., Sun, J., Xia, Y., Fonseca Rodrigues, M.-T., Vinod, S., Zhong, J., Chopra, N., et al. (2017). Carbon dioxide hydrogenation over a metal-free carbon-based catalyst. ACS Catal. *7*, 4497–4503.

5. Li, S., Xu, Y., Chen, Y., Li, W., Lin, L., Li, M., Deng, Y., Wang, X., Ge, B., Yang, C., et al. (2017). Tuning the selectivity of catalytic carbon dioxide hydrogenation over iridium/cerium oxide catalysts with a strong metal–support interaction. Angew. Chem. Int. Ed. Engl. *56*, 10761–10765.

6. Wesselbaum, S., vom Stein, T., Klankermayer, J., and Leitner, W. (2012). Hydrogenation of carbon dioxide to methanol by using a

homogeneous ruthenium–phosphine catalyst. Angew. Chem. Int. Ed. Engl. *51*, 7499–7502.

7. Aziz, M.A.A., Jalil, A.A., Triwahyono, S., and Ahmad, A. (2015). CO 2 methanation over heterogeneous catalysts: recent progress and future prospects. Green Chem. *17*, 2647–2663.

8. Polanski, J., Siudyga, T., Bartczak, P., Kapkowski, M., Ambrozkiewicz, W., Nobis, A., Sitko, R., Klimontko, J., Szade, J., and Lelątko, J. (2017). Oxide passivated Ni-supported Ru nanoparticles in silica: a new catalyst for low-temperature carbon dioxide methanation. Appl. Catal. B *206*, 16–23.

9. Kwak, J.H., Kovarik, L., and Szanyi, J.n. (2013). CO2 reduction on supported Ru/Al2O3 catalysts: cluster size dependence of product selectivity. ACS Catal. *3*, 2449–2455.

10. Tahir, M., Tahir, B., Amin, N.A.S., and Muhammad, A. (2016). Photocatalytic CO2 methanation over NiO/In2O3 promoted TiO2 nanocatalysts using H2O and/or H2 reductants. Energy Convers. Manag. *119*, 368–378.

11. Mateo, D., Albero, J., and García, H. (2017). Photoassisted methanation using Cu 2 O nanoparticles supported on graphene as a photocatalyst. Energy Environ. Sci. *10*, 2392–2400.

12. Jia, J., Wang, H., Lu, Z., O'Brien, P.G., Ghoussoub, M., Duchesne, P., Zheng, Z., Li, P., Qiao, Q., Wang, L., et al. (2017). Photothermal catalyst engineering: hydrogenation of gaseous CO2 with high activity and tailored selectivity. Adv. Sci. *4*, 1700252.

13. O'Brien, P.G., Ghuman, K.K., Jelle, A.A., Sandhel, A., Wood, T.E., Loh, J.Y.Y., Jia, J., Perovic, D., Singh, C.V., Kherani, N.P., et al. (2018). Enhanced photothermal reduction of gaseous CO 2 over silicon photonic crystal supported ruthenium at ambient temperature. Energy Environ. Sci. *11*, 3443–3451.

14. Zhao, Y., Zhao, B., Liu, J., Chen, G., Gao, R., Yao, S., Li, M., Zhang, Q., Gu, L., and Xie, J. (2016). Oxide-modified nickel photocatalysts for the production of hydrocarbons in visible light. Angew. Chem. Int. Ed. Engl. *128*, 4287–4291.

15. Ren, J., Ouyang, S., Xu, H., Meng, X., Wang, T., Wang, D., and Ye, J. (2017). Targeting activation of CO2 and H2 over Ru-loaded ultrathin layered double hydroxides to achieve efficient photothermal CO2 methanation in flow-type system. Adv. Energy Mater. *7*, 1601657.

16. Alsabeh, P.G., Rosas-Hernández, A., Barsch, E., Junge, H., Ludwig, R., and Beller, M. (2016). Iron-catalyzed photoreduction of carbon dioxide to synthesis gas. Angew. Chem. Int. Ed. Engl. *6*, 3623–3630.

17. Yang, H., Wu, Y., Lin, Q., Fan, L., Chai, X., Zhang, Q., Liu, J., He, C., and Lin, Z. (2018). Composition tailoring via N and S co-doping and structure tuning by constructing hierarchical pores: metal-free catalysts for high-performance electrochemical reduction of CO2. Catal. Science Technol. *57*, 15476–15480.

18. Mateo, D., Albero, J., and García, H. (2018). Graphene supported NiO/Ni nanoparticles as efficient photocatalyst for gas phase CO2 reduction with hydrogen. Appl. Catal. B *224*, 563–571.

19. Albero, J., Dominguez, E., Corma, A., and García, H. (2017). Continuous flow photoassisted CO 2 methanation. Sustain. Energ. Fuels *1*, 1303–1307.

20. Zhang, H., Wang, T., Wang, J., Liu, H., Dao, T.D., Li, M., Liu, G., Meng, X., Chang, K., Shi, L., et al. (2016). Surface-plasmon-enhanced photodriven CO2 reduction catalyzed by metal–organic-framework-derived iron nanoparticles encapsulated by ultrathin carbon layers. Adv. Mater. *28*, 3703–3710.

21. O'Brien, P.G., Sandhel, A., Wood, T.E., Jelle, A.A., Hoch, L.B., Perovic, D.D., Mims, C.A., and Ozin, G.A. (2014). Photomethanation of gaseous CO2 over Ru/silicon nanowire catalysts with visible and near-infrared photons. Adv. Sci. *1*, 1400001.

22. Jelle, A.A., Ghuman, K.K., O'Brien, P.G., Hmadeh, M., Sandhel, A., Perovic, D.D., Singh, C.V., Mims, C.A., and Ozin, G.A. (2018). Highly efficient ambient temperature CO2 photomethanation catalyzed by nanostructured RuO2 on silicon photonic crystal support. Adv. Energy Mater. *8*, 1702277.

23. Goto, Y., Hisatomi, T., Wang, Q., Higashi, T., Ishikiriyama, K., Maeda, T., Sakata, Y., Okunaka, S., Tokudome, H., Katayama, M., et al. (2018). A particulate photocatalyst water-splitting panel for large-scale solar hydrogen generation. Joule *2*, 509–520.

24. Chiang, T.H., Lyu, H., Hisatomi, T., Goto, Y., Takata, T., Katayama, M., Minegishi, T., and Domen, K. (2018). Efficient photocatalytic water splitting using al-doped SrTiO3 coloaded with molybdenum oxide and rhodium–chromium oxide. ACS Catal. *8*, 2782–2788.

25. Wang, M., Zheng, D., Ye, M., Zhang, C., Xu, B., Lin, C., Sun, L., and Lin, Z. (2015). One-dimensional densely aligned perovskite-decorated semiconductor heterojunctions with enhanced photocatalytic activity. Small *11*, 1436–1442.

26. Tan, H., Ye, E., and Fan, W.Y. (2006). Alumina-template synthesis of fluorescent RuO2 nanotubes derived from Ru3(CO)12 clusters. Adv. Mater. *18*, 619–623.

27. Xie, K., Umezawa, N., Zhang, N., Reunchan, P., Zhang, Y., and Ye, J. (2011). Self-doped SrTiO3−δ photocatalyst with enhanced activity for artificial photosynthesis under visible light. Energy Environ. Sci. *4*, 4211–4219.

28. O'Brien, P.G., Sandhel, A., Wood, T.E., Jelle, A.A., Hoch, L.B., Perovic, D.D., Mims, C.A., and Ozin, G.A. (2014). Photomethanation of gaseous CO2 over Ru/silicon nanowire catalysts with visible and near-infrared photons. Adv. Sci. *1*, 1400001.

29. Mateo, D., Albero, J., and García, H. (2017). Photoassisted methanation using Cu2O nanoparticles supported on graphene as a photocatalyst. Energy Environ. Sci. *10*, 2392–2400.

30. Zhao, P., He, Y., Cao, D.B., Wen, X., Xiang, H., Li, Y.W., Wang, J., and Jiao, H. (2015). High coverage adsorption and co-adsorption of CO and H2 on Ru(0001) from DFT and thermodynamics(0001) from DFT and thermodynamics. Phys. Chem. Chem. Phys. *17*, 19446–19456.

31. Morgan, D.J. (2015). Resolving ruthenium: XPS studies of common ruthenium materials. Surf. Interface Anal. *47*, 1072–1079.

32. Vasquez, R.P. (1992). SrTiO3 by XPS. Surf. Sci. Spectra *1*, 129–135.

33. Lingampalli, S.R., Ayyub, M.M., and Rao, C.N.R. (2017). Recent progress in the photocatalytic reduction of carbon dioxide. ACS Omega *2*, 2740–2748.